Catal Lett (2012) 142:195–204
DOI 10.1007/s10562-011-0747-3

Fischer–Tropsch Synthesis over Ordered Mesoporous Carbon Supported Cobalt Catalysts: The Role of Amount of Carbon Precursor in Catalytic Performance

Yifei Yang · Litao Jia · Yan Meng · Bo Hou · Debao Li · Yuhan Sun

Received: 13 September 2011 / Accepted: 15 November 2011 / Published online: 13 December 2011

Abstract Ordered mesoporous carbon supported cobalt-based catalysts (Co/MC) were synthesized via incipient wetness impregnation with different amounts of furfuryl alcohol (FA) as carbon precursor. The characterizations of obtained Co/MC were subjected to N_2 adsorption, XRD, XPS, TEM, H_2-TPR, H_2-TPD and H_2-TPSR. The results indicate that the reducibility and dispersion of Co active species vary significantly due to the difference of FA amount. By simply tuning the FA content from 25 to 100 wt%, the reduction temperature of deriving metallic Co shifts gradually to lower. The catalytic performance of Co/MC was evaluated for Fischer–Tropsch (FT) synthesis. The observed FT activity exhibits a volcano-type curve with the amount of FA due to the effect of both reducibility and dispersion of active species. As the precursor concentration overweighs 50 wt%, the ability of CO to dissociate over the active surface and the selectivity to the C_{5+} products level off after experiencing an initial increase. Substantially, the catalysts with higher concentration of FA render the larger crystallites having an average size of more than 6 nm, which facilitates the CO hydrogenation by way of carbon chain propagation. It seems that the sample with FA content of 50 wt% is optimum in terms of FT activity and C_{5+} selectivity.

Keywords Fischer–Tropsch synthesis · Ordered mesoporous carbon · Cobalt catalyst · Carbon precursor · Textural structure

Y. Yang · L. Jia (✉) · B. Hou · D. Li · Y. Sun (✉)
State Key Laboratory of Coal Conversion, Institute of Coal Chemistry, The Chinese Academy of Sciences, Taiyuan 030001, Shanxi, China
e-mail: jialitao910@163.com

Y. Sun
e-mail: yhsun@sxicc.ac.cn

Y. Yang
Graduate University of Chinese Academy of Sciences, Beijing 100049, China

Y. Meng · Y. Sun
Low Carbon Conversion Center, Shanghai Advanced Research Institute, The Chinese Academy of Sciences, Shanghai 201203, China

1 Introduction

Due to the depletion of oil resources and upgrading of environmental protection in recent years, Fischer–Tropsch synthesis (FTS) is increasingly becoming one of the promising chemical routes to convert coal or natural gas-derived syngas (a mixture of CO and H_2) to environmentally benign fuels and useful chemicals [1–5]. Cobalt catalysts are well-known for FTS due to their higher activity, higher selectivity for linear hydrocarbons, and lower water–gas shift activity for high ratio of H_2/CO in comparison with Fe-based catalysts [2]. At the conditions favoring chain growth, i.e., high C_{5+} selectivity, the cobalt catalyst activity is expected to be proportional to the number of surface cobalt metal (Co^0) sites. The final density of surface Co^0 sites depends on two main parameters, i.e., cobalt dispersion and reduction degree of supported cobalt oxide species [6, 7].

To enhance the density of surface-active sites (Co^0), high cobalt dispersion has been generally adopted by dispersing cobalt precursor on supports with high surface area. Among many kinds of supports, periodical mesoporous materials, especially silica-based solids, have attracted much attention [8–11]. The very high surface area

characteristics of mesoporous materials favor higher cobalt dispersion compared to conventional silica supports especially at high cobalt content. Moreover, the adjustable and uniform pore size distribution (PSD) of supports represents an effective approach to control the supported cobalt particle size and thus catalytic performance. Khodakov et al. [8] addressed that the mesoporous support with larger pore size was beneficial to higher FT reaction rate and C_{5+} selectivity which were ascribed to a higher reducibility of larger Co_3O_4 particles formed in the bigger pores of mesoporous silica supports. Xiong et al. [12] also reported that the large pore in mesoporous silica SBA-15 support significantly affected catalytic behavior and resulted in higher C_{5+} selectivity than counterpart with smaller pore size. In addition to the texture of mesoporous support, the interaction between the active phase and the support may also significantly affect the catalytic behaviors. Too weak an interaction may lead to a poor cobalt dispersion but relative high reducibility, whereas too strong an interaction will cause difficulty in the reduction but high cobalt dispersion [6]. Thus, it is crucial to balance the interaction between the support and cobalt precursor or active phase for FTS. Major drawback of conventional oxide support (SiO_2, Al_2O_3) is their reactions toward cobalt to form mixed oxides (silicate or aluminate) at a relatively low loading [13], which are hardly reducible to Co^0 and thus not active in FT reaction [14, 15]. Comparatively, carbon-based materials with inert surface properties may possibly overcome these difficulties. The inertness of carbon surface weakens the interaction between support and active phase and facilitates the reduction of cobalt precursor to Co^0. Accordingly, carbon supported cobalt catalysts were recently proposed as model systems for mechanism studies in FTS [16].

Ordered mesoporous carbon (OMC), derived from mesoporous silica inherits ordered pore structure and high surface area from their parent. Very recently, considering the intrinsic inertness and stability, OMC from mesoporous silica SBA-15 has been employed to support Ru for FTS [17]. As Ru particles were inside the channels or in carbon frameworks, the OMC supported Ru catalysts gave different performance for FTS. Similar to the mesoporous oxide support, the textural property of OMC is expected to influence the physico-chemical properties and catalytic performance of supported catalysts. Therefore, a careful tuning of the texture of OMC could provide a good approach to design a novel catalyst with optimal active site densities.

In the present work, we present a comprehensive study on the preparation and FTS performance of cobalt catalysts supported on a series of ordered mesoporous carbon materials (Co/MC). The texture of mesoporous carbon supports was carefully tuned by using different amounts of furfuryl alcohol (FA) as carbon precursor. Characterizations of Co/MC catalysts were performed by N_2 adsorption, X-ray diffraction (XRD), X-ray photoelectron spectroscopy (XPS), transmission electron microscopy (TEM), temperature-programmed reduction (TPR), H_2 temperature-programmed desorption (TPD) and temperature-programmed surface reaction (TPSR). The catalytic performances of Co/MC catalysts for FTS were investigated by using a fixed bed reactor.

2 Experimental

2.1 Catalyst Preparation

A series of ordered mesoporous carbons with different amounts of FA as carbon precursor were synthesized according to the previously reported method using SBA-15 (purchased from the Fudan University) as a hard template by incipient wetness impregnation (IWI) [18]. In a typical synthesis, a certain amount of FA (AR, Aladdin) dissolved in the trimethylbenzene (TMB, AR, Sinopharm) was used as the carbon precursor, and oxalic acid (AR, Sinopharm) was added to the FA solution as the polymerization catalyst. The FA solution was allowed to infiltrate into the SBA-15 channels at room temperature, followed by polymerization at 333 K and then at 353 K each for 16 h under ambient atmosphere. Afterwards, these composites were treated at 423 K for 3 h, and then heated to 573 K with a ramp of 2 K/min under argon atmosphere. Finally, the temperature continued being elevated to 1,173 K with a heating rate of 5 K/min and was maintained for 6 h to completely carbonize composites. The generated black powders were leached with HF (40%, AR, Kermel) aqueous solution to remove the silica, and further recovered by filtration, purged with distilled water and alcohol, and dried at 373 K to produce ordered mesoporous carbon powders. By adjusting the amounts of FA in TMB solutions, the derived mesoporous carbons were denoted as MC-X, with X = 25, 50, 70,100 representing 25, 50, 70,100 wt% FA in the starting TMB solutions. Before serving as supports, the MC-X was refluxed in concentrated HNO_3 (50%) at 353 K for 2 h.

Co/MC was obtained by sequential IWI using aqueous solutions of cobalt nitrate. At the beginning, five sequential cycles were adopted to disperse the active species on the supports. 3 g of different supports were completely wetted with deionized water to evaluate the corresponding volume. Then, 2.79 g of cobalt nitrate (AR, Kermel) was dissolved into the required deionized water to impregnate the supports. The catalysts were then dried under vacuum at the pressure of 0.09 MPa and temperature of 333 K and calcined in a flow of argon at 673 K

for 6 h. For the purpose of comparison, a reference catalyst 15Co/SBA-15 was prepared following the same procedure. Each catalyst is designated as 15Co/MC-X, where X represents the weight ratio of FA in the TMB solutions.

2.2 Catalyst Characterization

Nitrogen sorption was measured with an ASAP2010 Micromeritics instrument at liquid nitrogen temperature to obtain specific surface area, pore volume and PSD. Before the measurements, all the samples were degassed at 523 K for 6 h. The Brunauer–Emmett–Teller (BET) method was utilized to calculate the specific surface areas (S_{BET}) using adsorption data in a relative pressure range from 0.04 to 0.2. The pore volumes and PSD were derived from the adsorption branches of isotherms by using the Barrett–Joyner–Halenda (BJH) model. The total pore volume, V_t, was estimated from the adsorbed amount at a relative pressure P/P_0 of 0.985.

X-ray diffraction patterns were obtained at room temperature on a Rigaku D/maxRA diffractometer with a monochromatized Cu K_α radiation. Small-angle XRD data was collected from 0.5° to 5° (2θ) with a resolution of 0.02°. The wide-angle XRD spectra were scanned at a rate of 2.0°/min in the range $2\theta = 10$–$90°$. The average size of cobalt particles was estimated from the Scherrer equation using the most intense reflection at $2\theta = 42.2°$

$$d = \frac{k\lambda}{B\cos\theta}\frac{180^\circ}{\pi} \tag{1}$$

where d is the mean crystallite diameter, k (0.89) is the Scherrer constant, λ is the X-ray wave length (1.54056 Å) and B is the full width half maximum (FWHM) of the CoO diffraction.

The XPS spectra were recorded using a Physical Electronics PHI-5800 spectrometer with a monochromatized Al K-α source (1486.6 eV). The C 1s line (284.6 eV) from carbon support was taken as a reference to correct electrostatic charging. The measurements were performed at room temperature in high vacuum (10^{-8} Torr).

The reduction profiles of Co/MC catalysts were measured by H_2 temperature-programmed reduction (H_2-TPR). The experiment was performed in a U-tube quartz microreactor heated by an electrical furnace. The reactor was loaded with 30 mg of calcined catalyst. Prior to the H_2-TPR measurement, the calcined catalysts were flushed with high purity argon at 423 K for 1 h, and then cooled down to 323 K. Then, a gas consisting of 5% H_2 in Ar was switched on and temperature was increased at a ramp of 10 K/min from 323 to 1,233 K with a flow rate of 60 mL/min. The H_2 consumption was monitored in a thermal conductivity detector (TCD) and calibrated by reduction of identical mass ultrahigh-purity CuO (99.9999%) between RT and 1,233 K with the same heating rate. The extent of Co reduction was then calculated from the amount of H_2 consumed at temperature below 673 K. Assuming the complete reduction of CuO to Cu, the corresponding area of hydrogen consumption was achieved and further correlated with that of catalysts to estimate reducibility.

Hydrogen chemisorption measurements were carried out by using a Micromeritics Autochem 2910. 30 mg of the calcined catalyst was reduced at 673 K for 10 h and then cooled to 323 K under hydrogen flow. Then the flow of hydrogen was switched to argon at the same temperature, which lasted for about 30 min in order to remove the physisorbed hydrogen. Afterwards, the temperature programmed desorption (TPD) of the samples was obtained by increasing the temperature to 673 K under the argon flow with a ramp rate of 10 K/min. The resulting TPD spectra were used to determine the cobalt dispersion and average crystallite size. The dispersion and particle diameter were calculated according to the following formula [19, 20]:

$$\text{Calibration value (1 gas area units)} = \frac{\text{loop volume} \times \%\text{analytical gas}}{\text{mean calibration area} \times 100} \tag{2}$$

$$\text{H}_2\text{ uptake (mol/g cat.)} = \frac{\text{analytic area from TPD} \times \text{calibration value}}{\text{sample weight} \times 24.5} \tag{3}$$

$$\%\text{Dispersion} = \frac{\text{H}_2\text{ uptake} \times \text{cobalt atomic weight} \times \text{stoichiometry}}{\text{weight percentage}} \tag{4}$$

$$\text{Diameter} = \frac{6,000}{\text{active metal density} \times \text{monoatomic arranged area} \times \text{dispersion}} \tag{5}$$

Temperature-programmed surface reaction (TPSR) experiments were conducted on the same apparatus in H_2-TPD experiment as described above. 100 mg of sample was reduced in a flow of H_2 at 673 K for 10 h, and then purged by a flow of argon at the same temperature for 0.5 h. CO was adsorbed by a flow of 5% CO–Ar mixture (10 mL/min) at ambient temperature for 30 min. Physisorbed CO was purged with a He flow for 30 min. Finally, a flow of 10% H_2-Ar (20 mL/min) was passed through the catalyst bed when the temperature was increased with a ramp of 10 K/min from 300 to 1,173 K. MS signal at m/z = 15 (CH_4) was recorded.

Transmission electron microscopy (TEM) characterization of the samples was carried out by using a FEI Tecnai G2 instrument operating at a voltage of 200 kV. The samples were crushed in an agate mortar, ultrasonically dispersed in ethanol and deposited on a copper grid. The average particle size was evaluated from particle size histograms using the following formula:

$$d(3,2) = \frac{\sum_i N_i d_i^3}{\sum_i N_i d_i^2} \quad (6)$$

where N_i is the number of particles with d_i diameter.

2.3 Evaluation of Fischer–Tropsch Performance

FT reaction tests were carried out in a fixed bed tubular reactor, using 2 mL of fresh catalyst mixed with 2 mL of diluting material (SiO_2), which was inert for FT and acted as a good thermal conductor to control the process temperature. The catalysts were reduced in a flow of hydrogen at 673 K for 6 h and then cooled down to ambient before switching to syngas, which came from the methanol decomposition and consisted of 64.4 vol.% H_2, 31.9 vol% CO and 3.7 vol% N_2. Data was taken at steady-state after 24 h on-stream. The gas effluents were analyzed on-line by using a GC-8A chromatograph equipped with TCD and flame ionization detector (FID). Liquid products and wax were collected in a cold trap of 273–278 K and a hot trap of 373 K, respectively, and then were off-line analyzed on a GC-920 chromatograph, which was equipped with a 35mOV-101 capillary column. The carbon and mass balances were maintained in the range of 100 ± 5%.

3 Results and Discussion

3.1 Nitrogen Physisorption Measurements

Nitrogen physisorption at 77 K was used to evaluate the textural structure of supports and corresponding catalysts as well as the purchased parent SBA-15 (see Figs. 1, 2 and Table 1). In Fig. 1, it can be seen that all of MC supports exhibit typical type-IV hysteresis curves according to the IUPAC classification, indicating the presence of mesopores. The PSD of all MC supports are well-defined and approximately center at 4 nm. As listed in Table 1, the specific surface area of support decreases with an increase in FA amount, consistent with the results of Refs. 18 and 21. Among all the supports, MC-25 possesses the highest specific surface area of 895 m^2/g and the largest pore volume of 0.97 cm^3/g. As the FA concentration is increased to 100 wt%, the surface area and pore volume of MC decrease to 213.5 m^2/g, 0.2 cm^3/g, respectively. Cobalt infiltration results in the significant decrease of total pore volume and specific surface area of supports as well as the increase of mean pore diameter, which is probably

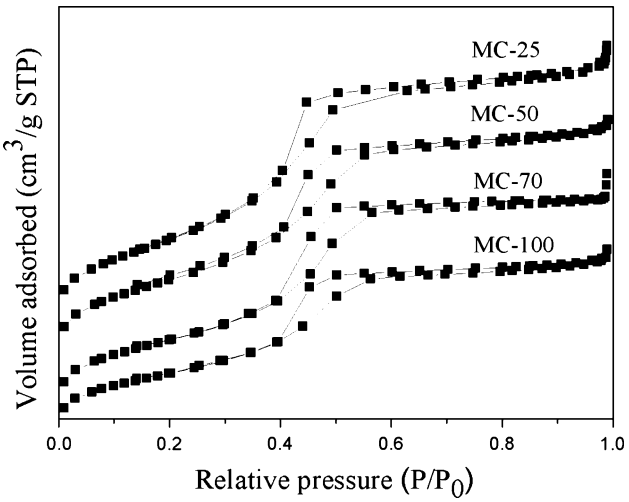

Fig. 1 Nitrogen physisorption of as-synthesized mesoporous carbon. The mesoporous carbon MC-50, MC-70, MC-100 were vertically offset by 100, 200, 300 cm^3/g STP, respectively

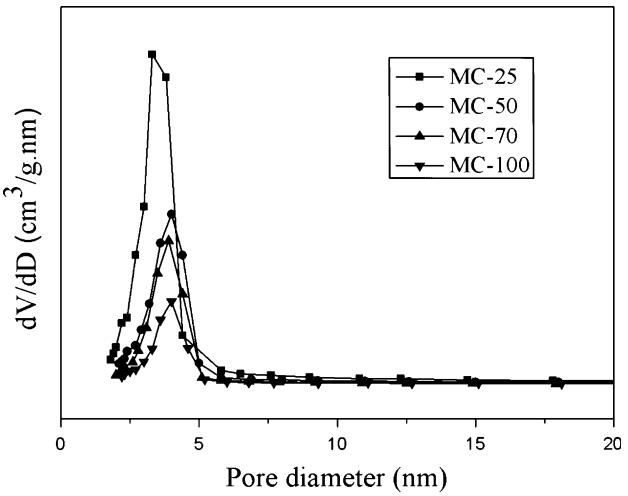

Fig. 2 Pore size distribution curve of as-synthesized mesoporous carbon

Table 1 Texture parameters of mesoporous carbons and corresponding catalysts

Sample	Total surface area (m^2/g)	Total pore volume (cm^3/g)	Average pore diameter (nm)
MC-25	895.65	0.97	3.82
MC-50	519.18	0.50	4.00
MC-70	378.71	0.39	4.28
MC-100	213.54	0.20	4.30
Co/MC-25	403.22	0.48	4.78
Co/MC-50	351.98	0.36	4.35
Co/MC-70	245.49	0.11	4.76
Co/MC-100	129.89	0.09	5.66
SBA-15	582.99	0.91	7.5

caused by partial blockage of mesoporous carbon channels by cobalt oxide clusters and/or partial collapse of mesoporous structure to form the packing pore [22].

3.2 Transmission Electronic Microscopy

The TEM observation of mesoporous carbons supported cobalt was carried out to probe the morphology and distribution of cobalt clusters in the resultant catalysts. Figure 3 reveals typical TEM images, together with CoO particle size distribution histograms which were extracted by directly measuring 100 particles from several TEM images to estimate the mean diameter of clusters.

The morphological observations (Fig. 3) of supported catalysts, to some extent, indicate that the catalyst particles are dispersed on the surface of support. For 15Co/MC-25, the average size of abundant particles which adhere to the channels of MC is in the range of 2–4 nm and parallels the average inner diameter of ca. 4 nm, accounting for the efficient confinement of mesochannel. While the FA content increases gradually, the positions of observed particles shift to outer surface. The inset histograms depicting the size distribution of particles show that by increasing the FA concentration from 25 to 100 wt%, the average cobalt particle size of supported catalysts increases from 4 to 11 nm.

3.3 X-Ray Powder Diffraction

The XRD patterns at low and high diffraction angles of the calcined samples in an argon flow are displayed in Figs. 4 and 5. The average crystallite size of cobalt oxide is calculated and compiled in Table 2.

The four distinct mesoporous carbons display a well-resolved (100) peak in Fig. 4, which is similar to the highly ordered 2D hexagonal mesostructure (P6mm) of SBA-15 template [23], and indicates a successfully inverse replica of hexagonal structure consisting of nanotube or nanorod after being subjected to a high-temperature calcination [18]. The presence of the diffraction peaks located at 2θ of 36.4°, 42.2° and 61.2° in Fig. 5 are indicative of cubic cobalt oxide (JFACDS file, No. 65-2902). However, many sources in the literature have reported that when aqueous solutions of cobalt nitrate were impregnated on SiO_2 or Al_2O_3, and followed by calcination at high temperature, Co_3O_4 was found to be the dominant phase of cobalt species [24]. To better address the formation of CoO, a mesoporous silica SBA-15 supported cobalt precursor calcined in the inert atmosphere was prepared and characterized by XRD as shown in Fig. 5. When the support is switched from mesoporous carbon to mesoporous silica, the corresponding active phase also transforms from CoO to Co_3O_4 indicating the argon treatment with poor contribution to generate CoO phase. In a sense, the results of MC supported catalysts might involve the participation of certain groups on the surface of mesoporous carbon as a reducing agent to induce reduction of Co_3O_4 to CoO in accordance with the previous result of activated carbon supported cobalt catalyst [25]. The higher the FA amount used in the preparation is, the stronger the XRD intensity of CoO in the resulting argon-treated catalyst is, and the narrower the FWHM of CoO diffraction peak is, the larger the formation of crystallites on the surface of supports is. According to the mean crystallite size calculated in Table 2, the detected average particle size is slightly smaller than that of TEM analysis but a similar changing rule. Concomitant with the gradual increase in FA content, the particles located in the supports are likely to undergo an agglomeration to crystallize and form the larger clusters.

3.4 X-Photoelectron Spectroscopy

X-photoelectron analysis was used in attempt to attain more insight into the surface composition of mesoporous carbon supported catalysts. The XPS spectra of Co 2p regions for the catalysts are illustrated in Fig. 6. The surface composition of the catalysts is quantified by binding energy of the Co 2p3/2 splitting-orbit at ca. 781 eV for each of catalyst, elucidating CoO as the predominant cobalt phase in these catalysts after calcination [24], which is also evidenced by XRD. In addition, a low intensity of shake-up satellite peak observed at ca. 787 eV is considered to be high-spinning Co^{2+} as the main form of cobalt species in the obtained composites, due to the absence of a shake-up process for low-spinning Co^{3+} ion (typical presence of $Co^{3+}/Co^{2+} = 2$ in Co_3O_4). Therefore, the surface valence state of as-synthesis catalysts primarily performs in the form of Co^{2+}.

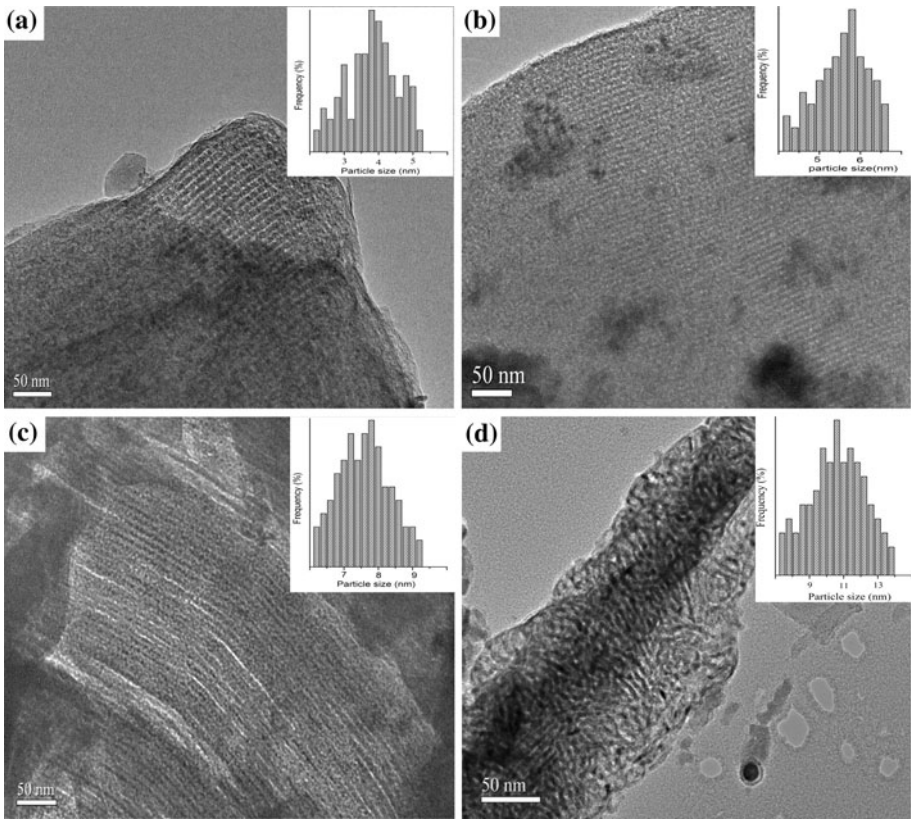

Fig. 3 TEM micrographs of calcined catalysts: **a** 15Co/MC-25; **b** 15Co/MC-50; **c** 15Co/MC-70; **d** 15Co/MC-100. The *inset* is the *histogram* of particle size distribution

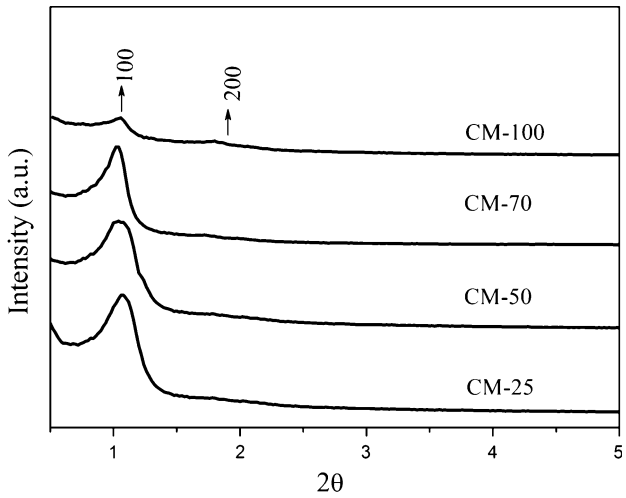

Fig. 4 The small-angle XRD patterns of mesoporous carbon supports

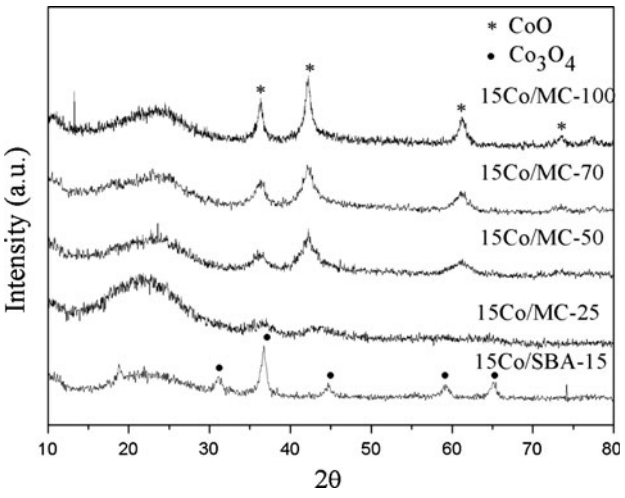

Fig. 5 The wide-angle XRD patterns of calcined catalysts

3.5 Temperature Programmed Reduction

The influence of FA amount on reduction behavior of catalysts was studied by TPR (see Fig. 7 and Table 2). For better distinguishing the reduction behavior of carbon supports, the performance of pristine mesoporous carbon under reduction conditions is also presented in the Fig. 7. The reduction curve of support is labeled as MC-X due to identical behavior for all the supports. As seen in Fig. 7, all of the catalysts exhibit multiple reduction peaks in the range of 600–1,000 K, which indicates the presence of a number of reduction steps of cobalt species [26]. According to the results of XRD and XPS, the presence of cobalt species on the catalysts principally performs in the form of CoO phase. Thus, the major reduction peak at ca. 720 K in the profile is assigned to the stage from CoO to metallic Co. Nevertheless, the satellite peak at 660 K for the catalyst 15Co/MC-50 and 15Co/MC-100 is probably attributed

Table 2 Characterization results of mesoporous carbon supported cobalt catalysts

Catalyst	Co^0 dispersion (%)	Reducibility (%)	Particle size (nm)			No. of active site $\times 10^{20}$
			d_{CoO}[a]	d_{CoO}[b]	d_{Co}[c]	
15Co/MC-25	19.52	58.68	2.83	4.02	4.91	1.75
15Co/MC-50	17.82	69.43	5.30	6.06	5.68	1.89
15Co/MC-70	12.68	76.49	6.63	7.92	7.51	1.44
15Co/MC-100	10.22	88.66	10.02	11.01	9.39	1.39

[a] The size of CoO particle estimated from the XRD pattern

[b] The obtained size of CoO particle based on the TEM analysis

[c] The reduced Co^0 particle size calculated from the H_2-TPD

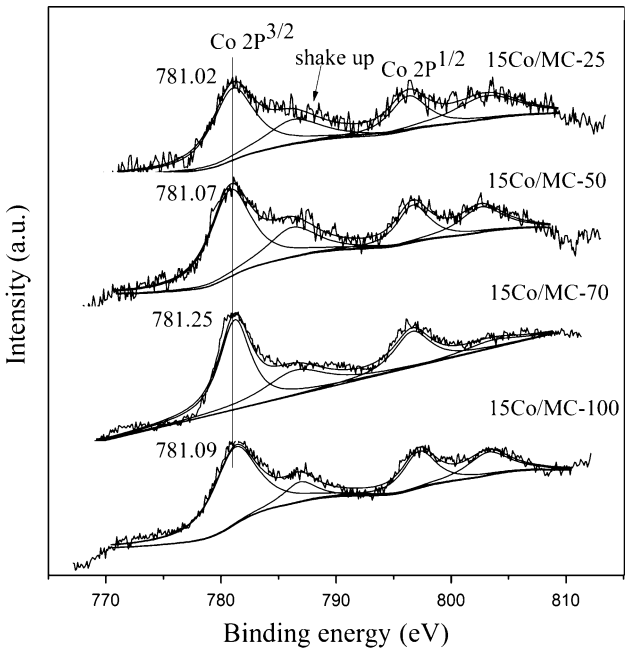

Fig. 6 The Co 2p XPS spectra of the prepared catalysts

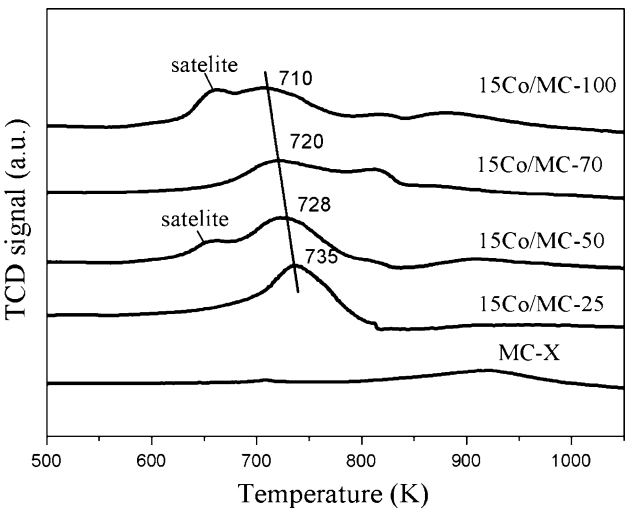

Fig. 7 TPR profiles for mesoporous carbons supported cobalt

to the reduction from Co_3O_4 to CoO [7], although no long-range ordered Co_3O_4 phase is detected in XRD. However, the broad peaks on the catalysts (ca. 800–1,073 K) are ascribed to the formation of methane originated from the reduction of the surface functional group on the mesoporous carbon in comparison with that of supports [27, 28], or the high-temperature reduction due to the specific interaction between active species and supports. Actually, the precise identity of the species is impossible and is just speculated as the results of a strong interaction between small cobalt oxide cluster and supports, whose properties deviate from the bulk-like cobalt oxides and need to be reduced in the higher temperature than the bulk oxides. Interestingly, the reduction temperature from CoO to metallic Co stage shifts gradually to lower value with the increase of FA concentration. The phenomenon could be interpreted that the increase in FA concentration results in increasing cluster size and weakening the interaction between active phase and electron-modified surface of supports, whose three-dimensional structures compose of nanotube or nanorod with graphite-like sheets enriching electron on the curvaceous surface [29], or the reaction-derived vapor induces the re-oxidation of small nanoparticles and delays the reduction temperature [30]. Consequently, the variance of FA concentration modifies the reduction behavior of surface cobalt species, which significantly induces the change of reducibility as shown in Table 2 [6].

3.6 H_2 Temperature-Programmed Desorption

The dispersion and particle size were estimated from H_2 TPD of the calcined catalysts in Table 2. For each sample, the obtained dispersion was based on the total amount of cobalt species in the samples. As it can be seen from Table 2, the increase of FA amount causes a pronounced increase in metallic cobalt particle size (i.e., decrease in dispersion), which is ascribed to the agglomeration of the cobalt crystallites leading to the decrease in the gross amount of active component atom exposed to external surface of cobalt clusters.

3.7 Temperature Programmed Surface Reaction (TPSR)

The reactivity of chemisorbed CO under H_2 flow could provide useful information about the ability to dissociate and hydrogenate of the catalyst over metallic cobalt surface [31]. Once surface-active carbon species are hydrogenated to methane, the formed methane is immediately released from the active surface and the corresponding desorption temperature and peak area are used to evaluate the dissociation and hydrogenation of CO. Figure 8 displays the H_2-TPSR spectra of adsorbed CO on mesoporous carbon supported cobalt catalysts. There are two primary methane peaks in H_2-TPSR spectra of all the catalysts. The CH_4 peak at low temperature indicates the formation of one type of carbon species from chemisorbed CO. Whereas, the one at high temperature is designated as the interaction between hydrogen and the different surface oxygen-containing groups on the mesoporous carbon surface and the hydrogenation of chemisorbed CO to yield methane [32], which is also observed in the TPR experiment. Since the FT reaction is operated at a relatively low temperature, the dissociation peak in high-temperature region does not likely contribute to FT synthesis. It is believed that the desorption of methane at low temperature is closely related to the activity of CO hydrogenation, which shifts to higher temperature firstly and then levels off with increasing FA concentration, as shown in Table 3. The trend is commensurate with the synergistic effect of reducibility and dispersion of active component on the supported catalysts. Meanwhile, it also verifies the effect of large particles diluting the capability of CO disassociation. The quantitative area of methane formation peak in low-temperature range increases smoothly with an increase in FA content,

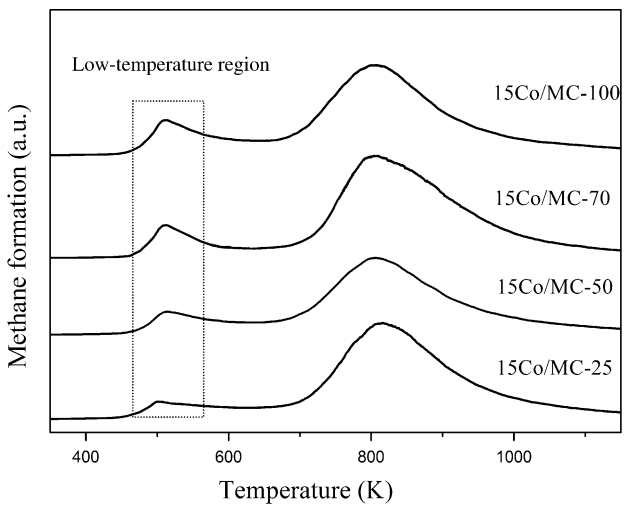

Fig. 8 TPSR spectra of adsorbed CO over the mesoporous carbon supported catalysts

Table 3 The result of TPSR spectra of adsorbed CO in the low-temperature region

Catalyst	Desorbed temperature (K)	Peak area $\times 10^{-9}$ (arbitrary unit)
15Co/MC-25	501	9.42
15Co/MC-50	512	12.21
15Co/MC-70	513	14.81
15Co/MC-100	511	19.50

which further demonstrates that the supports with higher precursor concentration derived larger crystallites are in favor of the propagation of carbon chain by means of CO hydrogenation.

3.8 Catalytic Results of the FTS Reaction

The catalytic activity of the different mesoporous carbon supported catalysts was evaluated by using a fixed-bed reactor under typical FTS conditions: 523 K, 2 MPa, $H_2/CO = 2$, and GHSV of 1,000 h^{-1}. The activity and selectivity results of FT reaction during the steady-state period were summarized in Table 4. The chain growth probability, alpha, was obtained from the slope of the Anderson–Shultz–Flory (ASF) plots in the C_{10}–C_{40} hydrocarbon range.

Figure 9 clarifies the dependence of CO conversion and C_{5+} selectivity on FA amount. The trend in variation of CO conversion undergoes a maximum at FA concentration of 50 wt% and then gradually decreases with increasing FA concentration. In principle, the activity of reduced Co catalysts is proportional to the concentration of surface Co^0 sites and irrespective of the support type [33]. However, the volcano-shaped curve observed in the present study thus reflects a difference with the trend of cobalt dispersion and extent of reduction when tuning the FA content. To better account for the interesting phenomenon, the number of active cobalt sites is introduced to comprehensively understand the influence of dispersion and reducibility, which is defined as [34] :

$$\text{No. of active sites} = \frac{\text{weigh of Co} \times \text{reducibility} \times \text{dispersion} \times N_A}{M_w} \quad (7)$$

where N_A is Avogadro's number and M_W is molecular weight of cobalt. The calculated results are presented in the Table 2. The number of active cobalt sites displays a remarkable increase, passes through a maximum at FA content of 50 wt% and then starts to decrease with increasing FA amount, which further verifies that conversion strongly depends on the number of active cobalt sites. In the case of 15Co/MC-25 catalyst with best dispersion among as-synthesized catalysts, the low activity is assigned

Table 4 FTS results of mesoporous carbon supported catalysts

Catalysts	CO conversion (%)	C_{5+}(STY) (g/mL/h)	Hydrocarbon distribution (wt%)			CO_2 selectivity (wt%)	ASF (α)
			CH_4	C_{2-4}	C_{5+}		
15Co/MC-25	34.00	0.034	30.37	18.92	50.70	3.77	0.726
15Co/MC-50	45.07	0.056	24.60	11.31	64.09	2.22	0.874
15Co/MC-70	37.80	0.047	24.16	12.89	62.94	1.67	0.819
15Co/MC-100	33.17	0.045	24.71	11.48	63.81	0.82	0.880

Reaction condition: $T = 523$ K, $H_2/CO = 2$, GHSV = 1,000 h^{-1}, $P = 2.0$ MPa

either to the changes in surface structure with lowest particle size or to electronic modifications as a result of more intimate interactions between the small crystallites and the support [8]. Furthermore, the small nanoparticles could be easily reoxidized by water and other reaction products at the conditions of FT synthesis [30], and the formation of oxides results in the low activity and high CO_2 selectivity. While the FA concentration surpasses 50 wt%, the magnitude of active species involved in the bulk phase overweighs the extent of reduction under hydrogen atmosphere. The formed specific structure renders unavailability to the adsorption and dissociation of CO and simultaneously weakens the activity of FT and the oxidation of large active particles. As a result, the corresponding CO_2 selectivity also decreases with increasing FA content in Table 4.

As seen in Fig. 9 and Table 4, the selectivity of C_{5+} hydrocarbons climbs up at first stage and then levels off with an increase in FA amount. For the catalyst 15Co/MC-25, the highest methane selectivity and lowest C_{5+} selectivity are observed. It is well known that the sizes of supported CoO crystallites can be modulated by the specific surface areas and pores of supports. According to TEM results, it is clear that most of the cobalt particles are dispersed on the interior surface as islands for catalyst 15Co/MC-25, while on the exterior surface for other counterparts. The featured location of cobalt clusters in 15Co/MC-25 results in the increase of H_2/CO ratio around the surface Co^0 sites, which is in favor of hydrogenation of the adsorbed species. Meanwhile, the low reducibility facilitates, at least in part, the formation of methane. In other words, the synergistic effect of high ratio of H_2/CO and the low reducibility leads to the higher methane selectivity and lower probability of carbon-chain propagation for catalyst 15Co/MC-25 in comparison with other catalysts. In the case of catalysts having FA concentration beyond 50%, the large cobalt particles on the external surface of catalysts expose to syngas and participate in the reabsorption of α-olefins which is extensively considered to be related with the chain-growing process and the formation of high molecular weight products [35–37]. Interestingly, it is found that the selectivity to C_{5+} hydrocarbons is independent of the change of FA content when that is more than 50 wt%. The similar rule is also observed for carbon nanofiber supported cobalt-based catalysts with particle size more than 6 nm [38], which might be caused by the steric hindrance for dissociative adsorption of CO and the $–CH_2–$ monomer and the low probability of addition of this monomer to the growing chain for large particles [33].

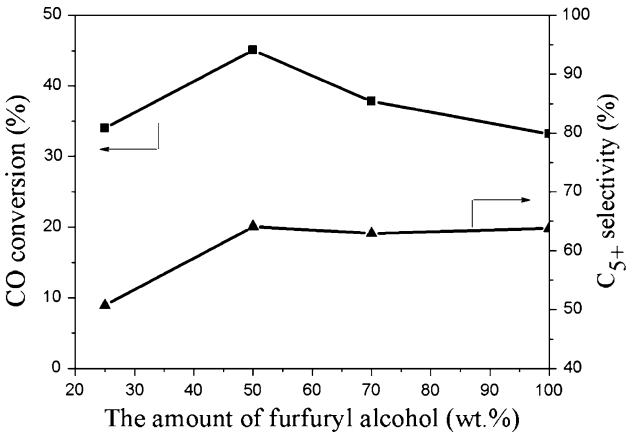

Fig. 9 The CO conversion and C_{5+} selectivity as a function of amount of FA

4 Conclusions

Ordered mesoporous carbon supported cobalt catalyst was successfully applied as a model catalyst to understand the effect of carbon precursor concentration on physicochemical property and catalytic performance during FTS. Just by simply tuning the precursor concentration of supports, the change of textural property of mesoporous carbon significantly results in different reducibility and dispersion of active species. With increasing FA content of the as-synthesized catalysts, the size of predominant phase CoO drastically increases. Meanwhile, the corresponding reduction temperature of deriving metallic Co decreases gradually due to the unique structure of mesoporous carbon. The observed FT activity exhibits a volcano-type curve with the increase of FA amount, which is attributed to the collaboration of reducibility and dispersion. While

the FA concentration is more than 50 wt%, the ability of CO dissociation over the active surface and the selectivity to the C_{5+} heavy molecular hydrocarbons level off and the generated large crystallites having size more than 6 nm are in favor of the propagation of carbon chain by means of CO hydrogenation. Therefore, the FA amount of 50 wt% would be an optimum for FT in terms of activity and C_{5+} selectivity. The design of mesoporous carbon supported Co catalysts with appropriate precursor concentration is possible a novel route to tune catalytic activity and selectivity to the desirable C_{5+} hydrocarbons.

Acknowledgments The work was supported by the National Natural Science Foundation of China (21003149 and 21076218).

References

1. Okabe K, Wei M, Arakawa H (2003) Energy Fuels 17:822
2. Yu ZX, Borg O, Chen D, Enger BC, Froseth V, Rytter E, Wigum H, Holmen A (2006) Catal Lett 109:43
3. Sun S, Tsubaki N, Fujimoto K (2000) Appl Catal A 202:121
4. MartInez A, López C, Márquez F, Diaz I (2003) J Catal 220:486
5. Sapag K, Rojas S, Granados ML, Fierro JLG, Mendioroz S (2001) J Mol Catal A 167:81
6. Jacobs G, Das TK, Zhang Y, Li J, Racoillet G, Davis BH (2002) Appl Catal A 233:263
7. Jacobs G, Ji Y, Davis BH, Cronauer D, Kropf AJ, Marshall CL (2007) Appl Catal A 333:177
8. Khodakov AY, Griboval-Constant A, Bechara R, Zholobenko VL (2002) J Catal 206:230
9. Prieto G, Martínez A, Murciano R, Arribas MA (2009) Appl Catal A 367:146
10. Yin D, Li W, Yang W, Xiang H, Sun Y, Zhong B, Peng S (2001) Microporous Mesoporous Mater 47:15
11. Mu S, Li D, Hou B, Jia L, Chen J, Sun Y (2010) Energy Fuels 24:3715
12. Xiong H, Zhang Y, Liew K, Li J (2008) J Mol Catal A 295:68
13. Wang W-J, Chen Y-W (1991) Appl Catal 77:223
14. Zhang J, Chen J, Ren J, Li Y, Sun Y (2003) Fuel 82:581
15. Zhang Y, Nagamori S, Hinchiranan S, Vitidsant T, Tsubaki N (2006) Energy Fuels 20:417
16. den Breejen JP, Radstake PB, Bezemer GL, Bitter JH, Frøseth V, Holmen A, Jong KPd (2009) J Am Chem Soc 131:7197
17. Xiong K, Li J, Liew K, Zhan X (2010) Appl Catal A 389:173
18. Lu A-H, Li W-C, Schmidt W, Kiefer W, Schüth F (2004) Carbon 42:2939
19. Trépanier M, Tavasoli A, Dalai AK, Abatzoglou N (2009) Appl Catal A 353:193
20. Rameswaran M, Bartholomew CH (1989) J Catal 117:218
21. Lu AH, Schmidt W, Schuth F (2003) New Carbon Mater 18:181
22. Li H, Wang S, Ling F, Li J (2006) J Mol Catal A 244:33
23. Zhao D, Feng J, Huo Q, Melosh N, Fredrickson GH, Chmelka BF, Stucky GD (1998) Science 279:548
24. Ernst B, Hilaire L, Kiennemann A (1999) Catal Today 50:413
25. Wang T, Ding YJ, Xiong JM, Yan L, Zhu HJ, Lu Y, Lin LW (2006) Catal Lett 107:47
26. Khodakov AY, Bechara R, Griboval-Constant A (2003) Appl Catal A 254:273
27. Guerrero-Ruiz A, Sepúlveda-Escribano A, Rodríguez-Ramos I (1994) Appl Catal A 120:71
28. Oades RD, Morris SR, Moyes RB (1990) Catal Today 7:199
29. Chen W, Fan Z, Pan X, Bao X (2008) J Am Chem Soc 130:9414
30. Grass ME, Zhang Y, Butcher DR, Park JY, Li Y, Bluhm H, Bratlie KM, Zhang T, Somorjai GA (2008) Angew Chem Int Ed 47:8893
31. Fujimoto K, Kameyama M, Kunugi T (1980) J Catal 61:7
32. Tsubaki N, Sun S, Fujimoto K (2001) J Catal 199:236
33. Iglesia E, Soled SL, Fiato RA (1992) J Catal 137:212
34. Tavasoli A, Sadagiani K, Khorashe F, Seifkordi AA, Rohani AA, Nakhaeipour A (2008) Fuel Process Technol 89:491
35. Kuipers EW, Scheper C, Wilson JH, Vinkenburg IH, Oosterbeek H (1996) J Catal 158:288
36. Tsubaki N, Yoshii K, Fujimoto K (2002) J Catal 207:371
37. Puskas I, Hurlbut RS (2003) Catal Today 84:99
38. Bezemer GL, Bitter JH, Kuipers H, Oosterbeek H, Holewijn JE, Xu XD, Kapteijn F, van Dillen AJ, de Jong KP (2006) J Am Chem Soc 128:3956